Journal of Catalysis **193,** 40–48 (2000)
doi:10.1006/jcat.2000.2875, available online at http://www.idealibrary.com on IDEAL®

Photocatalytic Water Splitting over Highly Donor-Doped (110) Layered Perovskites

Dong Won Hwang, Hyun Gyu Kim, Jindo Kim, Kyung Yong Cha, Young Gul Kim, and Jae Sung Lee[1]

Department of Chemical Engineering and School of Environmental Engineering, Pohang University of Science and Technology (POSTECH), San 31 Hyoja-dong, Pohang 790-784, Republic of Korea

Received July 30, 1999; accepted March 16, 2000

Highly donor-doped (110) layered perovskite materials loaded with nickel are efficient photocatalysts for overall water splitting with photon yields as high as 23% under UV irradiation. These novel photocatalysts are a series of homologous structures with a generic composition of $A_mB_mO_{3m+2}$ ($m = 4, 5$; $A =$ Ca, Sr, La; $B =$ Nb, Ti). The high electron density of these donor-rich materials would create a narrower charge depletion region of the semiconductor and an increased band bending, which allow more efficient electron-hole separation and higher quantum yields than undoped materials. Effects of catalyst preparation conditions are discussed on photocatalytic activity in water splitting.

Key Words: **photocatalyst; (110) layered perovskites; high donor concentration; overall water splitting.**

INTRODUCTION

Among various methods of solar energy conversion, much attention has been paid to photocatalytic water splitting for its potential significance in obtaining directly clean and high energy containing H_2 from abundant H_2O. If successfully developed with an economic viability, this could be the ultimate technology that could solve both energy and environmental problems altogether in the future. Since TiO_2 electrode was first studied for water decomposition under UV-light in 1972 (1), several efforts have been made to improve the catalytic activity. TiO_2-based photocatalysts such as Pt/TiO_2 and RuO_2/TiO_2 were investigated (2–4) and $SrTiO_3$-based photocatalysts such as a reduced $SrTiO_3$ electrode with a platinum counterelectrode, platinized $SrTiO_3$, $SrTiO_3$ powder modified by rhodium oxide, and nickel-loaded $SrTiO_3$ were also studied for improvement of their photocatalytic activities (5–8). However, quantum yields (% of absorbed photons that have been actually used to generate a photoreaction product) for these photocatalysts are very low (<1%). Recently, $K_4Nb_6O_{17}$ and $A_4Ta_xNb_{6-x}O_{17}$ ($A =$ K, Rb) with (100) layered structure showed much improved quantum yields of 5–10% (9–11). Quantum yields as high as 30% was obtained when $K_2La_2Ti_3O_{10}$ was prepared by the polymerized complex method (12). These layered materials use their interlayer space as reaction sites, where electron-hole recombination process could be retarded by physical separation of electron and hole pairs generated by photoabsorption. $BaTi_4O_9$ photocatalyst combined with RuO_2 was also reported to have a good activity for water decomposition due to their structural regularity of a tunnel structure, which could result in a high dispersion of RuO_2 over $BaTi_4O_9$ (13). $K_3Ta_3Si_2O_{13}$ was also found to be active for water splitting due to its pillared structure, under which energy transition could be facilitated since the binding angle of O–M–O–M–O of transition metal oxide structure with octahedral unit is nearly 180° (14). Recently, the same authors reported that nickel-doped $NaTaO_3$ showed a quantum yield of 28% under UV irradiation (15). However, it is desirable to find photocatalytic materials with even higher quantum yields in order for the water splitting to become a viable technology. Considering that materials with unique structures have good photocatalytic activities for water splitting, search for new photocatalysts with unique structural characteristics could be rewarding.

As mentioned earlier, perovskite materials such as $SrTiO_3$ and $CaTiO_3$ has received much attention in photocatalytic water splitting because of their improved photocatalytic activity compared with TiO_2 photocatalyst. Our novel photocatalysts (110) layered perovskite materials (16) are a series of homologous structures with a generic composition of $A_mB_mO_{3m+2}$ ($m = 4, 5$; $A =$ Ca, Sr, La; $B =$ Nb, Ti). Unlike the (100) layered materials reported by the Domen group (9–11), our materials have the perovskite slabs parallel to (110) relative to the perovskite structure and are highly donor-doped, because a five-valent element substitutes for a four-valent element or a three-valent element substitutes for a two-valent element in general perovskite materials such as $SrTiO_3$ and $CaTiO_3$ (17). The structural and electronic characteristics are believed to be responsible for the much improved quantum yields.

[1] To whom correspondence should be addressed. E-mail: jlee@postech.ac.kr.

0021-9517/00 $35.00

This paper is a detailed account of our Short Communication (16) and discusses structural and electronic characteristics of these novel photocatalysts together with their photocatalytic activities. Effects of catalyst preparation variables are also investigated on their catalytic performance in overall water splitting.

EXPERIMENTAL

For the preparation of photocatalysts a mixture of commercial metal oxides and carbonates in stoichiometric ratio was ground and pressed in the form of a pellet. Pellets were calcined at 1123–1173 K for 6 h and sintered at 1173–1623 K for 5 h in an electric furnace. For example, $Sr_2Nb_2O_7$ powder was prepared by heat treatment of the ground mixture of Nb_2O_5(99.9%, Aldrich) and $SrCO_3$(99.9%, Shinyo Pure Chem.) in a mole ratio of 1 to 2 at 1373 K for 5 h in air. The same method was applied for the other samples at following temperatures; $La_2Ti_2O_7$ at 1323 K from La_2O_3(99.9%, Aldrich) and TiO_2(99.9%, Aldrich), $Ca_2Nb_2O_7$ at 1173 K from $CaCO_3$(99.9%, Shinyo Pure Chem.) and Nb_2O_5, and $La_4CaTi_5O_{17}$ at 1273 K from La_2O_3, $CaCO_3$ and TiO_2. Metal (Ni, Pt, Cs, Bi, Fe, Pb, Ce)-loaded catalysts were prepared by an impregnation method: perovskite material was added in aqueous or nitric acid solution containing a required amount (0.01–5.0 wt% of powder) of a metal precursor (metal nitrate or chloride) and then was dried in an oven at 373 K and calcined at 573 K in air for 1 h. The metal-loaded catalysts were then pretreated in a closed gas circulation system; the sample was reduced by H_2 (22 μmol/s) at 673–1073 K for 2 h and then oxidized by air (22 μmol/s) at 473 K for 1 h.

The crystal structure of the sintered powder was determined by X-ray diffraction (XRD, Mac Science Co., M18XHF) and the band gap energy was measured by UV-Vis diffuse reflectance spectroscopy (Shimadzu, UV 525). The BET surface area was evaluated by N_2 adsorption in a constant volume adsorption apparatus (Micrometrics, ASAP 2012) and the morphology was determined by scanning electron microscopy (SEM, Hitachi, S-2460N). Transmission electron microscopy (TEM, Philips, CM 200) was used to observe the dispersion of the metal on the oxide powders. Temperature programmed reduction (TPR) experiment was performed to characterize the reducibility of metal-loaded catalysts; after purging a quartz catalyst bed containing 20 mg of sample with pure He at 373 K for 1 h, pure hydrogen was passed at a flow rate of 30 cc/min from 373 to 1273 K with a ramping rate of 10 K/min and the amount of H_2O evolved was measured by mass spectroscopy (HP 5890IIGC/5972MS detector).

Photocatalytic reaction was carried out at room temperature in a closed gas circulation system using a high-pressure Hg lamp (Ace Glass Inc., 450W) placed in an inner irradiation-type quartz reaction cell. The catalyst (1.0 g) was suspended in distilled water (500 ml) by magnetic stirring. The rates of H_2 and O_2 evolution were analyzed by gas chromatography (TCD, molecular sieve 5-Å column and Ar carrier).

The quantum yield of various photocatalysts was calculated by the chemical actinometer of potassium ferrioxalate ($K_3(Fe(C_2O_4)_3) \cdot 3H_2O$) (18). For the preparation of $K_3Fe(C_2O_4)_3 \cdot 3H_2O$, 1.5 M $K_2C_2O_4$ and 1.5 M $FeCl_3$ were mixed with stirring. The green precipitate was recrystallized three times in hot water and dried at 318 K. For the measurement of photon flux, 500 ml of 0.006 M $K_3Fe(C_2O_4)_3 \cdot 3H_2O$ was illuminated for 60 s and then the absorbance at 510 nm of the mixture of the illuminated solution and 1,10-phenanthroline indicator was measured in a cell of 1 cm length.

RESULTS

Characterization of $Sr_2Nb_2O_7$

Figure 1 shows the XRD pattern of $Sr_2Nb_2O_7$ fabricated by sintering the ground mixture of $SrCO_3$ and Nb_2O_5 at 1373 K for 5 h in air and the schematic structure of $Sr_2Nb_2O_7$. Below 1373 K there were many impurity phases and thus $Sr_2Nb_2O_7$ was synthesized by heat treatment at 1373 K. While the slabs in $K_4Nb_6O_{17}$, a member of (100)-layered materials, are obtained by cutting the perovskite

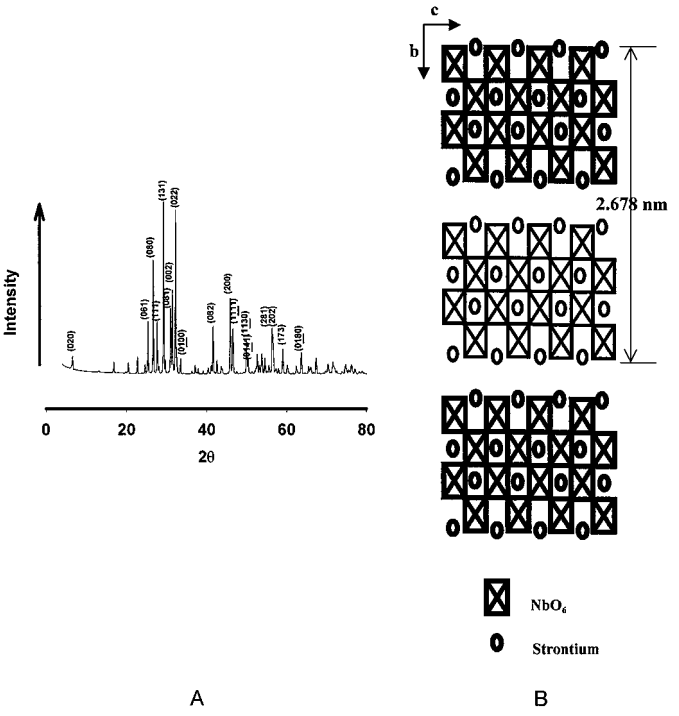

FIG. 1. (A) An XRD pattern of $Sr_2Nb_2O_7$ sintered in air at 1373 K for 5 h and (B) schematic structure of $Sr_2Nb_2O_7$: Perovskite-type slabs are idealized and the slabs in thick lines are shifted with respect to the others by a/z.

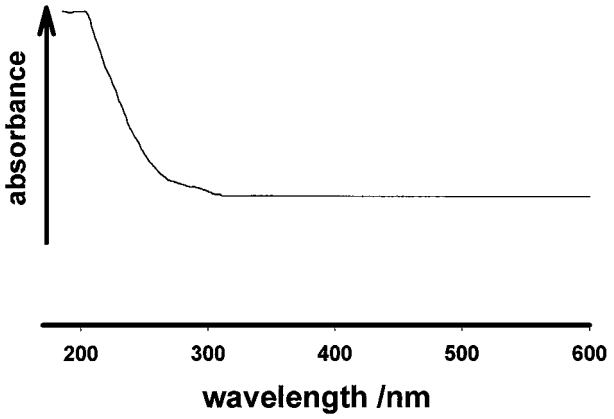

FIG. 2. The UV-DRS of $Sr_2Nb_2O_7$.

structure parallel to (100) planes (19, 20), those in $Sr_2Nb_2O_7$, a member of (110) layered perovskite, are obtained by cutting the perovskite structure parallel to (110) planes (21, 22). The slabs in thick lines are shifted with respect to the others by a/z. Replacing Ti^{4+} with Nb^{5+} in the common perovskite oxide $SrTiO_3$ forms this structure. The extra electron from niobium could serve as a donor. Thus, this material is in the donor-rich state, which results in distorted, cation-deficient, and oxygen-rich interlayer. Its lattice parameter was estimated to be $a = 3.955$ Å, $b = 26.78$ Å, and $c = 5.7$ Å.

From UV-Vis DRS spectrum of $Sr_2Nb_2O_7$ shown in Fig. 2, the band gap energy was estimated to be ca. 4.1 eV (<300 nm), which was larger than the energy required for water to be decomposed (>2.43 eV). BET surface area was small (5 m^2/g) due to the high temperature heat treatment (1373 K for 5 h). The average particle size after grinding the sintered material was estimated to be 5 μm from SEM photograph shown in Fig. 3. In Fig. 4, TEM image of 1 wt% nickel-loaded $Sr_2Nb_2O_7$ shows nickel particles well dispersed on $Sr_2Nb_2O_7$ with an average particle size of ca. 30 nm. This indicates that nickel is mostly deposited on outer surface of $Sr_2Nb_2O_7$.

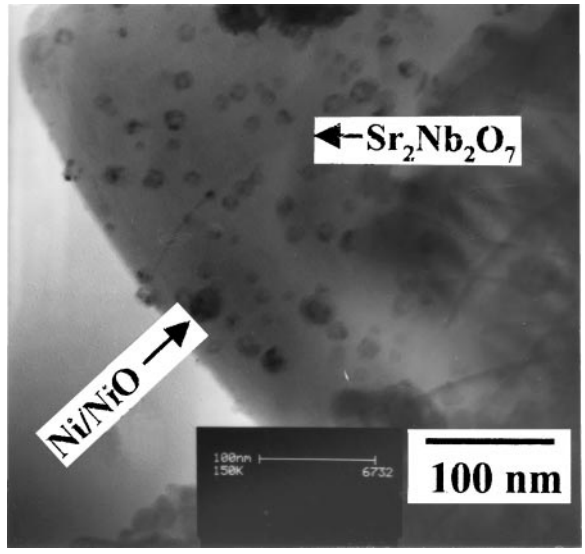

FIG. 4. The TEM image of Ni(1.0 wt%)/$Sr_2Nb_2O_7$. Catalyst was pretreated by reduction at 973 K for 2 h followed by oxidation at 473 K for 1 h.

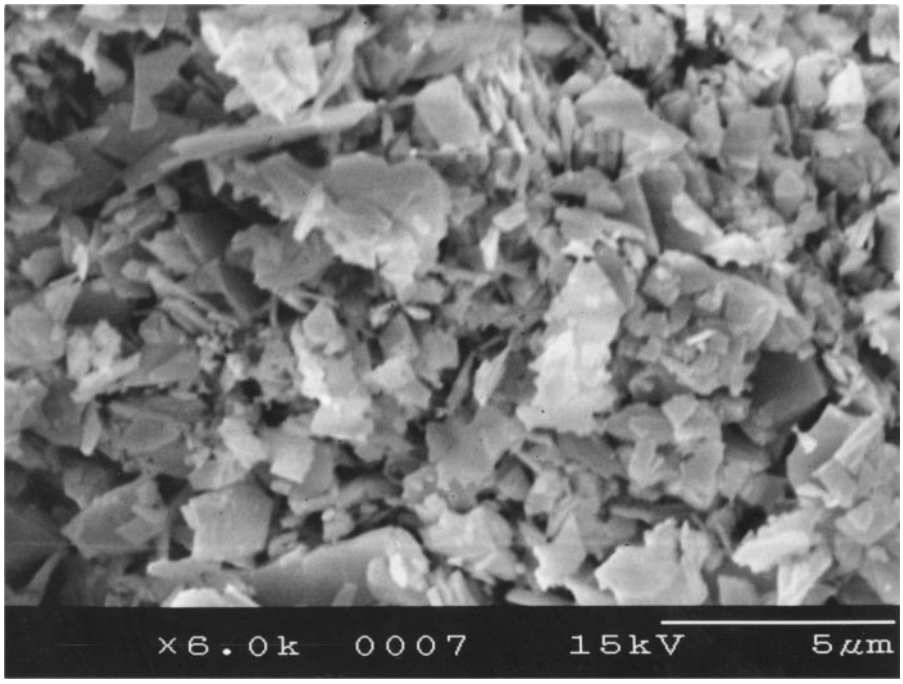

FIG. 3. The SEM image of $Sr_2Nb_2O_7$ sintered in air at 1373 K for 5 h.

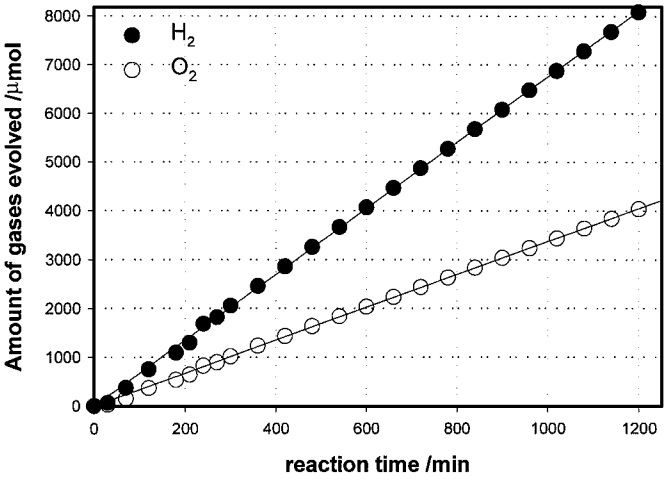

FIG. 5. A typical time courses of H_2 and O_2 evolution over Ni(1.0 wt%)/$Sr_2Nb_2O_7$. Catalyst was pretreated by reduction at 973 K for 2 h followed by oxidation at 473 K for 1 h. Reaction conditions: catalyst 1 g; distilled water 500 ml; light source: 450 W high-pressure Hg lamp placed in inner irradiation reaction cell.

Photocatalytic Water Decomposition over $Sr_2Nb_2O_7$ and Metal-Doped Catalysts

Figure 5 shows a typical time course of H_2 and O_2 gas evolution for the photocatalytic decomposition of water over Ni/$Sr_2Nb_2O_7$. The catalyst produces H_2 (402 μmol/h) and O_2 (198 μmol/h) in a stoichiometric ratio ($H_2 : O_2 = 2 : 1$). In early studies of water splitting, the simultaneous evolution of O_2 and H_2 (overall water splitting) had been a challenge due to the difficulty of O_2 formation and the rapid reverse reaction between the two products (23, 24). Furthermore, the reaction proceeds at a steady rate with no indication of catalyst deactivation for 20 h during which moles of H_2 produced (8087 μmol) are greater than moles of the catalyst by factors of ca. 50 for Ni (170 μmol) and ca. 2 for Nb (4534 μmol) contained in the whole catalyst (1 g). Since two electrons are needed to produce a molecule of H_2 from water, the latter corresponds to the turnover number of 4 if all Nb atoms have participated in the water splitting. This demonstrates that overall water splitting on this material proceeds catalytically. Table 1 summarizes the rate of H_2 evolution measured for 5 h over various catalysts. After the lamp reached its steady state, H_2 concentration increased linearly with time under UV irradiation over various metal-loaded catalysts and $Sr_2Nb_2O_7$ alone (10 μmol H_2/h). Of several metals, nickel showed the highest activity (288 μmol H_2/h) followed by Cs (94 μmol H_2/h). Platinum was known to be the best metal promoter for TiO_2 (3, 25), but it was ineffective for $Sr_2Nb_2O_7$.

Effects of Pretreatments and Nickel Loading

A proper pretreatment of metal-loaded catalyst was important to achieve the high activity especially for nickel-loaded catalysts as shown in Fig. 6. This marked dependence of photocatalytic activity on pretreatment conditions was not observed for other metal promoters. The oxidized form of Ni/$Sr_2Nb_2O_7$ treated in air at 773 K for 1 h, was more active than the reduced form treated in H_2 at 773 K for 2 h (180 μmol/h vs 90 μmol/h). The best result was obtained when the catalyst was first reduced at 773 K for 2 h and then oxidized at 473 K for 1 h (288 μmol/h). To examine the effect of pretreatments for nickel-loaded $Sr_2Nb_2O_7$, temperature programmed reduction (TPR) was carried out in H_2 flows (Fig. 7). A typical peak of nickel oxide around 723 K was observed for the oxidized catalyst (Fig. 7B) but no peak for the reduced catalyst (Fig. 7C). From this, it could be concluded that the oxidized form of nickel on $Sr_2Nb_2O_7$ was completely reduced after the reduction in H_2 at 773 K for

TABLE 1

H_2 Evolution Rate of $Sr_2Nb_2O_7$ and Metal-Loaded $Sr_2Nb_2O_7$ Catalysts[a]

Catalyst	Rate of H_2 Evolution / μmol h^{-1}
$Sr_2Nb_2O_7$	10
Pb(1.0 wt%)/$Sr_2Nb_2O_7$	10
Fe(1.0 wt%)/$Sr_2Nb_2O_7$	12
Pt(1.0 wt%)/$Sr_2Nb_2O_7$	14
Ce(1.0 wt%)/$Sr_2Nb_2O_7$	20
Bi(1.0 wt%)/$Sr_2Nb_2O_7$	44
Cs(1.0 wt%)/$Sr_2Nb_2O_7$	94
Ni(1.0 wt%)/$Sr_2Nb_2O_7$	288

[a] All catalysts were reduced by H_2 at 773 K for 2 h and oxidized by air at 473 K for 1 h: catalyst 1 g; distilled water 500 ml; light source: 450 W high-pressure Hg lamp placed in inner irradiation reaction cell.

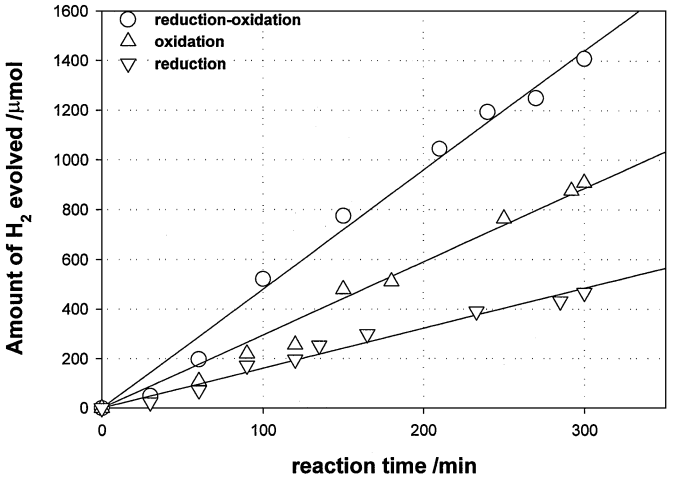

FIG. 6. Dependence of photocatalytic activity of Ni(1.0 wt%)/$Sr_2Nb_2O_7$ on pretreatment conditions. Reaction conditions: catalyst 1 g; distilled water 500 ml; light source: 450 W high-pressure Hg lamp placed in inner irradiation reaction cell.

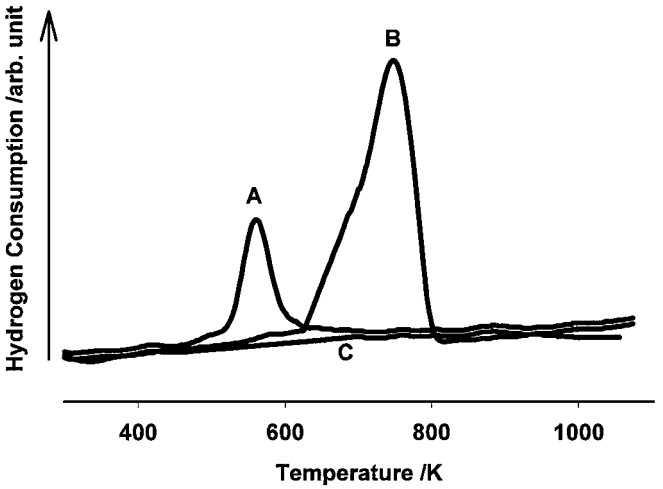

FIG. 7. The TPR profile of Ni(1.0 wt%)/$Sr_2Nb_2O_7$. (A) after reduction and oxidation, (B) after oxidation, and (C) after reduction.

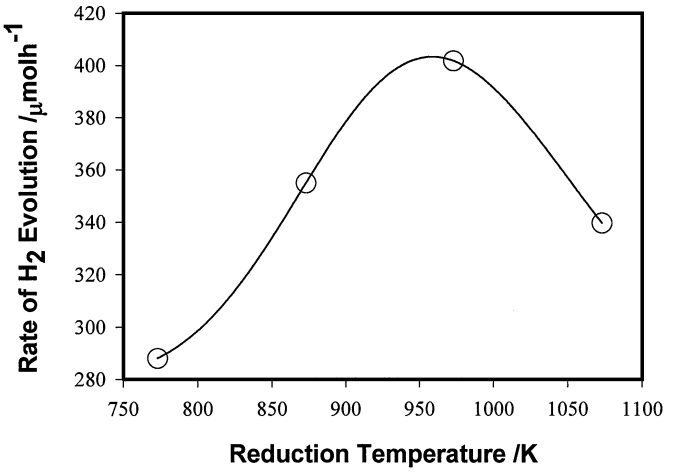

FIG. 9. Dependence of the activity of Ni(1.0 wt%)/$Sr_2Nb_2O_7$ on the reduction temperature. Reoxidation temperature was kept at 473 K for 1 h. Reaction conditions: catalyst 1 g; distilled water 500 ml; light source: 450 W high-pressure Hg lamp placed in inner irradiation reaction cell.

2 h. The catalyst subject to the reduction-oxidation treatment had a new peak around 573 K and its area covered only about 40% of the peak of the oxidized catalyst. Thus, the reduced surface of nickel was only partially oxidized and this partial oxidization of nickel surface might be important to activate the photocatalyst $Sr_2Nb_2O_7$.

Figure 8 shows that activity of nickel-loaded $Sr_2Nb_2O_7$ pretreated by reduction at 773 K for 2 h and then oxidization at 473 K for 1 h depends on the amount of nickel loading. Rates of H_2 evolution over Ni/$Sr_2Nb_2O_7$ increased with the amount of nickel loading up to 1.0 wt% of $Sr_2Nb_2O_7$ and then decreased at loading higher than 1 wt%. Thus, it was necessary to have an optimum level of nickel loading on $Sr_2Nb_2O_7$ for efficient water splitting.

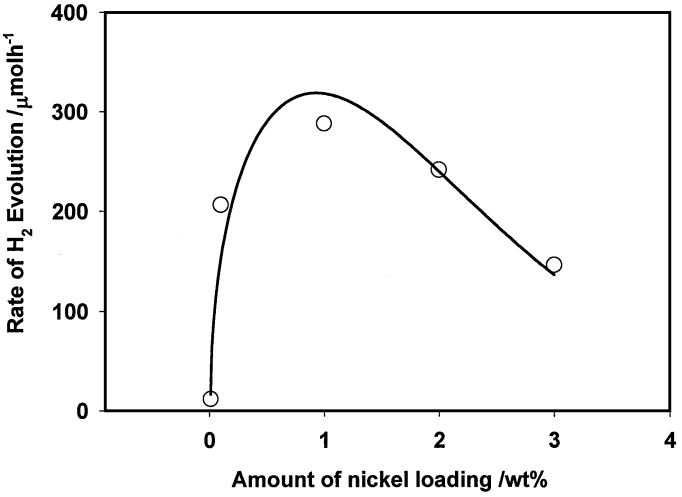

FIG. 8. Dependence of the photocatalytic activity of Ni/$Sr_2Nb_2O_7$ on nickel loadings. Catalyst was pretreated by reduction at 773 K for 2 h followed by oxidation at 473 K for 1 h. Reaction conditions: catalyst 1 g; distilled water 500 ml; light source: 450 W high-pressure Hg lamp placed in inner irradiation reaction cell.

As shown in Fig. 9, photocatalytic activity of Ni(1.0 wt%)/$Sr_2Nb_2O_7$ varied with the reduction temperature of nickel-loaded catalyst when reoxidization temperature was kept at 473 K. An optimal reduction temperature of 973 K was identified.

Effects of Solution pH and Sacrificial Agents

Modification of catalyst surface with hydroxyl group (OH^-) or hydrogen ion (H^+) could enhance its photocatalytic activity by changing the property of interface between catalyst and electrolyte. The adjustment of solution pH by adding H_2SO_4 or KOH was performed to change the property of the interface. The activity of Ni(1.0 wt%)/$Sr_2Nb_2O_7$ depended markedly on pH as shown in Fig. 10. First, there was no pH change at pH 7 when 1 g of Ni(1.0 wt%)/$Sr_2Nb_2O_7$ was added to 500 ml of distilled water, indicating that the catalyst was stable in aqueous solution. The rate of H_2 evolution increased with pH up to ca. 10 and then decreased drastically at the higher pH region. Thus, at the optimum solution pH of 10, H_2 was evolved about three times as fast as at pH 7 (1100 μmol/h vs 402 μmol/h). This phenomenon is often observed in water splitting over semiconductor photocatalysts and has been interpreted as the requirement of a certain amount of hydroxyl group to facilitate the desorption of O_2 generated before it is consumed in the reverse reaction ($H_2 + 1/2O_2 \rightarrow H_2O$) (5, 25). However, too much hydroxyl group (pH > 10) could retard H_2 desorption.

In overall water splitting, oxidation of water by holes is a slower process than reduction by electrons (23, 24). In order to facilitate the oxidation, hole-scavengers are often introduced. Thus 400 ml of distilled water and 100 ml of

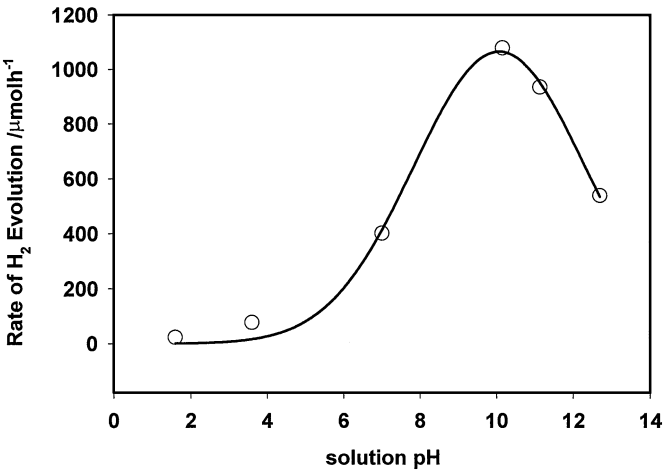

FIG. 10. Dependence of the activity of Ni(1.0 wt%)/$Sr_2Nb_2O_7$ on the solution pH. Catalyst was pretreated by reduction at 973 K for 2 h followed by oxidation at 473 K for 1 h. Reaction conditions: catalyst 1 g; distilled water 500 ml; light source: 450 W high-pressure Hg lamp placed in inner irradiation reaction cell.

alcohol (methanol, ethanol, or 1-propanol) containing 1 g of the catalyst was illuminated under otherwise identical reaction conditions and the results are shown in Fig. 11. When the solution without alcohol was illuminated, the rate of H_2 evolution was 288 μmol/h (E). When alcohol was included but catalyst was omitted, H_2 was evolved at a rate of 350 μmol/h (D). The three different alcohols gave the similar rates. Finally, when both alcohol and catalyst were used, the rate of H_2 evolution for methanol was 7400 μmol/h (A) and carbon dioxide was the product of alcohol oxidation, while oxygen was not evolved. Of three alcohols of

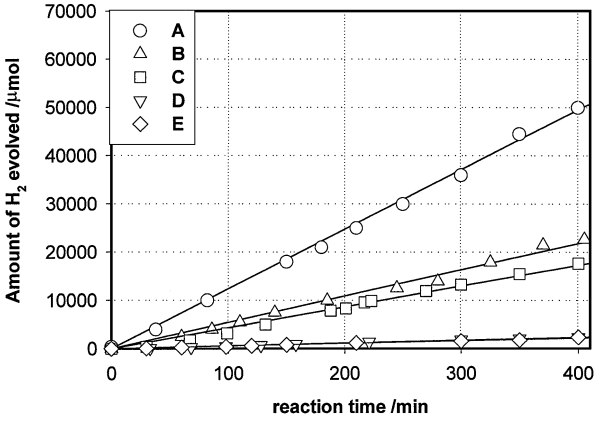

FIG. 11. Dependence of activity of Ni(1.0 wt%)/$Sr_2Nb_2O_7$ on the type of hole scavenger: (A) methanol 100 ml + catalyst 1 g, (B) ethanol 100 ml + catalyst 1 g, (C) 1-propanol 100 ml + catalyst 1 g, (D) methanol 100 ml without catalyst, and (E) catalyst 1 g without alcohol. Catalyst was pretreated by reduction at 773 K for 2 h followed by oxidation at 473 K for 1 h. Reaction conditions: catalyst 1 g; distilled water 400 ml + alcohol 100 ml; light source: 450 W high-pressure Hg lamp placed in inner irradiation reaction cell.

TABLE 2

Physical Properties, H_2 Evolution Rates, and Quantum Efficiency of Various Photocatalysts

Catalyst[a]	BET surface area/m^2g^{-1}	Band gap/eV	Rate of H_2 evolution/ μmol h^{-1}	Quantum Yield (%)
$Ca_2Nb_2O_7$	4.2	4.3	101	7 (<288 nm)
$Sr_2Nb_2O_7$	5.1	4.1	402	23 (<300 nm)
$La_2Ti_2O_7$	5.2	3.2	441	12 (<360 nm)
$La_4CaTi_5O_{17}$	4.9	3.8	499	20 (<320 nm)
$K_4Nb_6O_{17}$	4.5	3.3	210	5 (<360 nm)
$KBa_2Ta_3O_{10}$	4.2	3.5	150	8 (<350 nm)
$SrTiO_3$	4.0	3.2	30	0.81 (<360 nm)
$CaTiO_3$	4.0	3.5	16	0.85 (<350 nm)
TiO_2	50.0	3.1	0.3	$\ll$1 (<360 nm)

[a] (110) layered and perovskite materials were loaded with Ni(1.0 wt%) and then pretreated by reduction at 973 K for 2 h followed by oxidation at 473 K for 1 h and (100) layered materials were loaded with Ni(0.1 wt%) and then pretreated by reduction at 773 K for 2 h followed by oxidation at 473 K for 1 h, while TiO_2 was loaded with Pt(1.0 wt%) and pretreated by oxidation at 573 K for 2 h: catalyst 1 g; distilled water 500 ml; light source: 450 W high-pressure Hg lamp placed in inner irradiation reaction cell.

different chain sizes, methanol showed the highest hole-scavenging effect followed by ethanol (3200 μmol/h) (B) and 1-propanol (2600 μmol/h) (C).

Other (110) Perovskite Oxides

Table 2 summarizes the results of water decomposition and catalyst characterization for a number of photocatalysts. Our (110) layered catalysts ($Ca_2Nb_2O_7$, $Sr_2Nb_2O_7$, $La_2Ti_2O_7$ and $La_4CaTi_5O_{17}$) are compared with previously known (100) layered perovskite catalysts ($K_4Nb_6O_{17}$ and $KBa_2Ta_3O_{10}$), bulk-type perovskite ($SrTiO_3$, $CaTiO_3$), and bulk-type TiO_2 catalyst (Degusa P-25), all under the same reaction conditions. $La_4CaTi_5O_{17}$ is the second member of $A_mB_mO_{3m+2}$ with $m = 5$. All catalysts except TiO_2 were loaded with Ni, while Pt was loaded onto TiO_2 because Pt is known to be the best modifier for TiO_2. The BET surface areas of all photocatalysts fabricated by sintering are 4–5 m^2 g^{-1}, while that of TiO_2 P25 is 50 m^2 g^{-1}. The band gap energies estimated from UV-VIS diffuse reflectance spectra of all catalysts are in the 3.1–4.3 eV UV energy range.

It is clear that (110) layered perovskite catalysts are, as a group, much more active than previously reported perovskite material, $SrTiO_3$ and $CaTiO_3$, (100) layered material, $K_4Nb_6O_{17}$ and $KBa_2Ta_3O_{10}$, and bulk-type TiO_2 for the photocatalytic decomposition of water into H_2 and O_2 under UV irradiation. The rate of H_2 evolution over Pt/TiO_2 was a mere 0.3 μmol/h. Dramatic improvement is observed for Ni-doped perovskite material (30 μmol/h for $SrTiO_3$ and 16 μmol/h for $CaTiO_3$) and further for (100) layered material ($K_4Nb_6O_{17}$, $KBa_2Ta_3O_{10}$) and still further for (110) layered perovskites. The quantum yield is the more

meaningful parameter than the rate of H_2 evolution itself to gauge the performance of a photocatalyst because the rate is normalized against the absorbed photons. The photon flux from the UV lamp varies depending on the wavelength and, hence, the quantum yield is not necessarily proportional to the rate of H_2 production when semiconductors of different band gaps are used as catalysts. Yet, it is again clear that (110) layered perovskite materials are superior to previously known photocatalysts also in terms of the quantum yield. Although the quantum yield of ca. 30% has been already reported for $NiO/K_2La_2Ti_3O_{10}$ prepared by the polymerized complex method, quantum yield for that catalyst prepared by the conventional solid-state reaction was only 17% (12). Therefore, the quantum yield of 23% for $Sr_2Nb_2O_7$ by conventional solid-state reaction is much higher than general perovskites and other layered photocatalysts such as $K_4Nb_6O_{17}$ and $K_2La_2Ti_3O_{10}$ for overall water splitting. The quantum yield for 5% for $K_4Nb_6O_{17}$ is in agreement with the previous reports for the same material (10).

Catalyst Stability

For the batch reactor like ours, the pressure of reactor increases with reaction time since the product H_2 and O_2 from H_2O are evolved continuously with reaction time. This could be a barrier to efficient water decomposition because of the meaningless reverse reaction of H_2 and O_2 to H_2O. H_2 evolution rate decreased a little with reaction time but the initial activity was fully recovered after purging the reactor with N_2. Therefore, the reason for the small decrease of H_2 evolution rate was not the deactivation of the catalyst, but the increase in the reactor pressure by water decomposition. It was already mentioned that there was no pH change of the reaction solution during photocatalytic reactions. Furthermore as shown in Fig. 12, the XRD pattern of the catalyst before the reaction was identical to that after reaction of 10 h, indicating that these catalysts are stable under UV-light and in the aqueous medium.

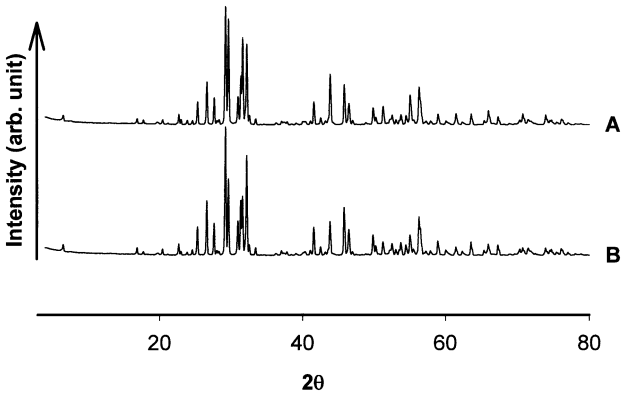

FIG. 12. XRD patterns of Ni(1.0 wt%)/$Sr_2Nb_2O_7$ before and after reaction. Catalyst was pretreated by reduction at 973 K for 2 h followed by oxidation at 473 K for 1 h and Reaction was proceeded for 20 h.

DISCUSSION

Novel photocatalysts reported here; i.e., (110) layered perovskite catalysts are much more active than previously known some (100) layered materials or bulk-type perovskite oxides for the photocatalytic decomposition of water into H_2 and O_2 under UV irradiation. In addition to these high activities, H_2 and O_2 are produced in a stoichiometric ratio ($H_2 : O_2 = 2 : 1$). There was no indication of catalyst deactivation for 20 h during which the catalyst has turned over many times making the process of overall water splitting catalytic.

Examination of quantum yields listed in Table 2 reveals that the superior performance of $A_mB_mO_{3m+2}$ ($m = 4, 5$) is general and not limited to one specific composition. Although these quantum yields are not the highest reported to date, there was a dramatic improvement compared with general perovskite materials such as $SrTiO_3$ and $CaTiO_3$. Probably, their structure is important for photocatalytic activity. If TiO_2 component of $CaTiO_3$ or $SrTiO_3$ with the ideal perovskite structure is completely replaced by Nb_2O_5, the product is $Ca_2Nb_2O_7$ or $Sr_2Nb_2O_7$. The replacement of Ti^{4+} by Nb^{5+} results in excess electrons and slabs of a distorted perovskite structure of m unit cells thick in order to accommodate excess oxygen (21). This also occurs when Ca^{2+} or Sr^{2+} is replaced by La^{3+} as in $La_2Ti_2O_7$. This structural substitution gives highly donor-doped (110) layered perovskite materials $A_4B_4O_{14}$, commonly denoted as $A_2B_2O_7$. When a part of oxygen is lost, the next structure in the series is obtained as in $La_4CaTi_5O_{17}$.

As mentioned, layered compound, $K_4Nb_6O_{17}$ or tunnel-structure compound, $BaTi_4O_9$ have received attention recently since they are much more active than bulk-type photocatalysts such as TiO_2 or $SrTiO_3$ with perovskite structure for photocatalytic water splitting. The high activity of these materials has been attributed to effective utilization of interlayer space as reaction sites. We have discovered that the (110) layered perovskites of $A_mB_mO_{3m+2}$ ($m = 4, 5$; A = Ca, Sr, La; B = Nb, Ti) are still more active with relatively high quantum yields. These novel photocatalysts are of a layered structure and hence one might expect the contribution of the interlayer space as reaction sites as in other types of layered materials as reported by Domen *et al.* Yet, it is known that the interlayer of these materials is not hydrated and both H_2 and O_2 evolution has to proceed only at the surface (26). Hence, we have to consider other factors to account for the further high quantum yields.

In photocatalytic water splitting over a semiconductor, excited electron-hole pairs are generated when the catalyst is illuminated with light having energy equal to or greater than the band gap. The principal challenge is how to

suppress the energy-wasteful recombination of the formed electron-hole pairs. Recombination is usually much more facile than subsequent steps needed for water cleavage. In a semiconductor–liquid interface, the electron-hole pairs are separated by electric field present in the depletion layer. It is expected that the highly donor-doped (110) perovskite would create a narrower depletion layer than undoped perovskite as is observed for metal-ion doped TiO_2 (27). Band bending would then take place on a depletion layer with a narrower width or become more drastic (28). Finally, the increased band bending would allow more efficient charge separation and enhance the overall quantum yield of water splitting.

Photocatalytic activity depended strongly not only on the electronic structure characterized by high donor concentration as discussed above but also on the loaded metal and pretreatment conditions. Thus, (110) perovskite materials themselves could not decompose water efficiently (quantum yields <1%) because substantial electron-hole recombination process could still occur. Of several metals loaded on (110) perovskite materials, nickel was found to be the most effective for water decomposition and this might also be due to the role of nickel in charge separation. This trend of nickel being the best modifier of our materials is consistent with that of $NiO/K_4Nb_6O_{17}$. Furthermore, these photocatalysts were further activated by pretreatments of reduction followed by oxidation in the same manner as with $NiO/K_4Nb_6O_{17}$ and $NiO/SrTiO_3$. However, the difference between $NiO/K_4Nb_6O_{17}$ and NiO/(110) layered perovskite materials is the position of nickel particle. Thus, nickel particles could not be intercalated into the interlayer space in our material unlike in $K_4Nb_6O_{17}$. Instead, nickel particles in our materials are deposited only on the external surface of these materials like in $NiO/SrTiO_3$ and $NiO/K_2La_2Ti_3O_{10}$ as shown in TEM image of nickel-loaded materials (Fig. 4). In our materials, nickel particles are on the external surface, while in $NiO/K_4Nb_6O_{17}$, nickel particles are intercalated into the interlayer space by the ion exchange of nickel precursor with potassium ion. Therefore, the mechanism of water splitting on our materials is expected to be similar to that for $NiO/SrTiO_3$ or $NiO/K_2La_2Ti_3O_{10}$, where nickel particles are deposited on the external surface of these materials.

This significant variation in photocatalytic activity for water splitting with loaded metal might be ascribed to the role of nickel in p–n junction between nickel and layered perovskite material as reported by Domen and Nozik (8, 29). Platinum was also reported to form ohmic junction with TiO_2 (30), but it was ineffective for our layered perovskites because platinum might not construct p–n junction with layered perovskite materials. Although this p–n junction was made possible by reduction at 773 K for 2 h followed by oxidation at 473 K for 1 h, further increase of photocatalytic activity was made possible when nickel-loaded catalyst was reduced at 973 K for 2 h and then oxidized at 473 K for 1 h. Thus, it could be concluded that the best p–n junction was formed by this pretreatments. Reduction at temperatures higher than 973 K could make the p–n junction collapse by segregation of nickel metal from (110) perovskite materials and photocatalytic activity decreases.

The photocatalytic activity increased with the amount of external dopant (nickel loading) up to 1 wt% but the further increase of nickel loading was detrimental to photocatalytic water splitting. As mentioned earlier, both nickel oxide, a p-type semiconductor, and the perovskite material, an n-type semiconductor, should absorb the sufficient photons needed for its band gap excitation so that the p–n junction can be operated properly. When this ratio was not optimized (nickel loading <1 wt% or >1 wt%), photocatalytic activity of catalyst was reduced.

Based on our understanding of nickel-loaded (110) perovskite materials, the sequence of water decomposition over Ni/NiO/(110) perovskite could be described as follows.

(1) photons are absorbed both in the slabs of (110) perovskite oxide and in nickel oxide; (2) a more efficient electron-hole separation takes place than in the undoped perovskite oxides (internal doping effect); (3) electron generated in the slabs of (110) perovskite is transferred to the p–n junction and hole generated in nickel oxide is transferred to the p–n junction (external doping effect); (4) reduction of H_2O takes place in Ni/NiO by electron and oxidation of H_2O takes place on the surface of (110) perovskite by hole.

CONCLUSION

Nickel-loaded (110) perovskite materials were found to be good photocatalysts as a group with high quantum yields and stoichometric evolution of H_2 and O_2 from H_2O was observed for all these materials. These high activities resulted from their layered structure and the high concentration of donor level compared with bulk type perovskite photocatalysts. When nickel was combined with these materials, and upon a proper pretreatment, a significant increase of photocatalytic activity was observed, which might be due to formation of a p–n junction between nickel oxide and perovskite materials. The reduction of water appeared to occur on the external surface of nickel oxide, while the oxidation of water on the surface of (110) perovskite.

REFERENCES

1. Fujishima, A., and Honda, K., *Nature (London)* **238**, 37 (1972).
2. Bulatov, A. V., and Khidekel, M. L., *Izv. Akad. Nauk SSSR Ser. Khim.* 1902 (1976).
3. Sato, S., and White, J. M., *Chem. Phys. Lett.* **72**, 83 (1980).
4. Kwai, T., and Sakata, T., *Chem. Phys. Lett.* **72**, 87 (1980).
5. Wagner, F. T., and Somorjai, G. A., *J. Am. Chem. Soc.* **102**, 5494 (1980).
6. Wrighton, M. S., Ellis, A. B., Wolczanski, P. T., Morse, D. L., Abrahamson, H. B., and Ginley, D. S., *J. Am. Chem. Soc.* **98**, 2774 (1976).

7. Lehn, J. M., Sauvage, J. P., Ziessel, R., and Hilaire, L., *Israel J. Chem.* **22**, 168 (1982).
8. Domen, K., Kudo, A., and Onishi, T., *J. Catal.* **102**, 92 (1986).
9. Domen, K., Kudo, A., Shinozaki, A., Tanaka, A., Maruya, K., and Onishi, T., *J. Chem. Soc. Chem. Commun.*, 356 (1986).
10. Sayama, K., Tanaka, A., Domen, K., Maruya, K., and Onishi, T., *J. Catal.* **124**, 541 (1990).
11. Sayama, K., Arakawa, H., and Domen, K., *Catal. Today* **28**, 175 (1996).
12. Ikeda, S., Hara, M., Kondo, J. N., Domen, K., Takahashi, H., Okubo, T., and Kakihana, M., *J. Mater. Res.* **13**, 852 (1998).
13. Inoue, Y., Asai, Y., and Sato, K., *J. Chem. Soc., Faraday Trans.* **90**, 797 (1994).
14. Kudo, A., and Kato, H., *Chem. Lett.*, 867 (1997).
15. Kato, H., and Kudo, A., *Catal. Lett.* **58**, 153 (1999).
16. Kim, H. G., Hwang, D. W., Kim, J., Kim, Y. G., and Lee, J. S., *Chem. Commun.*, 1077 (1999).
17. Ishizawa, N., Marumo, F., Kawamura, T., and Kimura, M., *Acta. Crystallogr. Sect. B* **31**, 1912 (1975).
18. Rabek, J. F., "Experimental Methods in Photochemistry and Photophysics," Part 2. Wiley, New York, 1982.
19. Ruddlesden, S. N., and Popper, P., *Acta. Crystallogr.* **10**, 54 (1958).
20. Dion, M., Gann, M., and Tournoux, M., *Mater. Res. Bull.* **16**, 1429 (1981).
21. Smyth, D. M., Liu, D., and Yao, X., *Mater. Res. Bull.* **27**, 387 (1992).
22. Smyth, D. M., in "Properties and Applications of Perovskite-Type Oxides" (L. G. Tejuca and J. L. G. Fierro, Eds.), pp. 47–72. Dekker, New York, 1993.
23. Millis, A., and Porter, G., *J. Chem. Soc. Faraday Trans. I* **78**, 3659 (1984).
24. Kiwi, J., and Grätzel, M., *J. Phys. Chem.* **88**, 6146 (1984).
25. Sato, S., and White, J. M., *J. Catal.* **69**, 128 (1981).
26. Kudo, A., Kato, H., and Nakagawa, S., *J. Phys. Chem. B* **104**, 571 (2000).
27. Kiwi, J., in "Homogeneous and Hetrogeneous Photocatalysis" (E. Pelizzetti and N. Serpone, Eds.), pp. 275–302. Reidel, Dordrecht, 1986.
28. Schiavwllo, M., and Sclafani, A., in "Photocatalysis: Fundamentals and Aplications" (N. Serpone and E. Pelizzetti, Eds.), p. 159. Wiley Interscience, New York, 1989.
29. Nozik, A. J., *Appl. Phys. Lett.* **30**, 567 (1977).
30. Gregory, A., and Allen, J. B., *J. Phys. Chem.* **87**, 1979 (1983).